Charged- and neutral-particle production from 400-GeV/c pp collisions

R. D. Kass,* W. Ko, R. L. Lander, W. Michael, D. E. Pellett, and P. M. Yager

University of California, Davis, Davis, California 95616

R. Ely, G. Gidal, and P. Hanson

Lawrence Berkeley Laboratory, Berkeley, California 94720

(Received 8 November 1978)

Charged- and neutral-particle production from 400-GeV/c pp collisions are measured simultaneously using the Fermilab 15-ft bubble chamber. The π^0 and K^0 cross sections are rising at Fermilab energies, while the Λ^0 cross section remains fairly constant. Similarly, the average number of π^0s and K^0s increases as a function of the number of negative particles in an event, yet no such dependence is noted for the Λ^0s. The ratio of average number of π^0 to average number of π^- per inelastic collisions is found to be constant at Serpukhov and Fermilab energies (40 to 400 GeV/c) and equal to 1.22 ± 0.02. Cross sections for Σ^0 and $\bar{\Sigma}^0$ production are measured and limits are found for η^0 and ω^0 production. Neutral- and charged-pion correlations are compared with five pion-production models.

I. INTRODUCTION

A great deal of work has been done on high-energy inclusive charged-particle production or neutral-particle production,[1] but seldom both in one experiment. To distinguish among various theoretical models, one generally needs the simultaneous measurement of charged and neutral particles. In this paper we present results on charged- and neutral-particle production from 400-GeV/c pp collisions in the Fermilab 15-ft bubble chamber, with emphasis on the inclusive and semi-inclusive production of π^0s, K_S^0s, Λ^0s, and $\bar{\Lambda}^0$s. Using the large number of γ's that convert to e^+e^- in the chamber liquid (5 to 10 times that in the Fermilab 30-inch chamber), we are able to measure the cross section for Σ^0 and $\bar{\Sigma}^0$ production and calculate upper limits for inclusive $\eta^0(548)$ and $\omega^0(783)$ production. Correlations between neutral and charged pions are studied in terms of $\langle \pi^0 \rangle_-$ and the Mueller moments f_2^{--}, f_2^{0-}, and f_2^{00}.

II. EXPERIMENTAL DETAILS

A. Scanning and measuring

The data of this experiment[2] were obtained from a 30 000-picture (5.9 μb/event) exposure of the 15-ft hydrogen bubble chamber to a 400-GeV/c proton beam.

Approximately 60% of the film was scanned at the University of California, Davis (UCD) and 40% at LBL using dual magnification scan tables with image-plane digitizers, on-line either to a microprocessor system (UCD)[3] or an IBM 7044 (LBL).

For each scannable frame the number of beam tracks was recorded. For each interaction the charged multiplicity and number of associated neutrals were recorded, and guidance points for

the measurement were digitized.

Approximately 12% of the film was scanned twice in order to estimate the efficiency for locating V^0's or γ's in a single event, and to estimate the efficiency of locating events in a frame. The efficiency for locating V^0's or γ's was determined for three types of events: events with ≤ 6 prongs (95 $\pm 1.4\%$), $6 <$ prongs ≤ 12 (90 $\pm 1.5\%$), and >12 prongs (88 $\pm 1.8\%$). The efficiency for finding primary interactions was determined separately for two prongs (90 $\pm 3\%$) and events with >2 prongs (99.4 $\pm 0.3\%$).

All events were measured with an LBL Franckenstein measuring device which utilized the CICERO[4] software-hardware package. All event measurements were processed using TVGP and SQUAW. Each track leaving a vertex was fitted with three different mass hypotheses, viz., π, K, or p for a primary vertex and e, π, or p for a secondary vertex. It was necessary to implement a vertex-finding algorithm in TVGP because a significant number of vertices were obscured by holes in the Scotchlite due to patches or the piston ring.

Tracks were rejected if the root-mean-square film residuals (FRMS) of the track were ≥ 21 μm or if the track failed to reconstruct in TVGP. Tracks with large FRMS (>21 μm for all mass interpretations) comprise 3.6% of the reconstructed tracks leaving the primary vertex and 5% of the reconstructed tracks leaving the secondary vertex. For tracks leaving the primary vertex we find that 2.8% of the tracks fail to reconstruct, while for tracks coming from a secondary vertex 2.2% fail to reconstruct. The measuring efficiency for tracks from the primary vertex is 91% while the efficiency for measuring a V^0/γ is 87%.

The fiducial volume for the primary vertex was chosen to be[5] $-180 \leq X \leq 152$ cm. The fiducial vol-

TABLE I. Listing of 3C-fit ambiguities. The P_T^- refers to the transverse momentum of the π^- when a K^0 is involved, π^- of Λ^0 for $\gamma\Lambda^0$ ambiguities, and $\bar{p}$ for $\gamma\bar{\Lambda}^0$ ambiguities. The overlap events are those events which have P_T^- of the V^0 > 20 MeV/c and P_T^- of the γ < 20 MeV/c.

P_T^- (MeV/c)	γK^0	$\gamma\Lambda^0$	$\gamma\bar{\Lambda}^0$	$K^0\Lambda^0$	$K^0\bar{\Lambda}^0$	$\Lambda^0\bar{\Lambda}^0$	$\gamma K^0\Lambda^0$	$\gamma K^0\bar{\Lambda}^0$	$\gamma\Lambda\Lambda^0$	$K^0\Lambda^0\bar{\Lambda}^0$	$\gamma K^0\Lambda^0\bar{\Lambda}^0$
0–20	51	57	85	0	0	0	4	3	0	0	1
20–40	5	16	8	0	0	0	2	1	0	0	0
40–102	8	52	10	10	5	0	13	8	0	0	0
102–206	57	0	0	3	0	0	12	6	0	0	0
Overlap	0	8	11	0	0	0	2	0	0	0	0
Totals	121	133	114	13	5	0	33	18	0	0	1

ume for secondary vertices was chosen to be

$$|X| \leq 160 \text{ cm},$$

$$|Y| \leq 160 \text{ cm},$$

and

$$|Z| \leq 75 \text{ cm},$$

ensuring that there is at least one foot (in space) of track for measurement. In addition, the minimum distance between the primary and secondary vertex was required to be greater than 4 (15) cm for V^0's (γ's).

B. Selection of three-constraint fits at the secondary vertex

The computer program SQUAW was used to attempt a three-constraint (3C) kinematical fit to the following reactions:

(1) $\gamma p \rightarrow e^+e^-p_s$, p_s = spectator proton

(2) $K_S^0 \rightarrow \pi^+\pi^-$,

(3) $\Lambda^0 \rightarrow p\pi^-$,

(4) $\bar{\Lambda}^0 \rightarrow \pi^+\bar{p}^-$.

Table I shows that for a sample of 3177 neutrals giving a 3C fit (confidence level >10^{-5}) approximately 14% of the neutrals fit two or more of the above reactions.

In order to resolve the V^0-γ ambiguities an event was called a γ if P_T^- for both the V^0 and γ hypothesis was ≤ 20 MeV/c. A smaller number of events (21) had P_T^- of the γ < 20 MeV/c, but P_T^- of the V^0 ≈ 20 MeV/c (overlap in Table I). These events were all classified as γ's. The γ sample is estimated to be at least 99% pure. To separate K^0's from Λ^0's and $\bar{\Lambda}^0$'s we require that P_T^- of the K^0 be >102 MeV/c. The K^0 sample is estimated to be at least 96% pure, while the Λ^0 sample is estimated to be at least 90% pure.

A neutral was considered to be a $\bar{\Lambda}^0$ candidate if it was assigned a $\bar{\Lambda}^0$ identity using the procedure that was outlined for the Λ^0's and was backward in

the center of mass. All $\bar{\Lambda}^0$ candidates were examined at the scan table. Using the scan information, $\bar{\Lambda}$-γ ambiguities were resolved in favor of the $\bar{\Lambda}^0$ if there was evidence of any of the following:

(1) A nonzero opening angle,

(2) decay of outgoing track,

(3) outgoing track interacts.

The $\bar{\Lambda}^0$-K^0 ambiguities were resolved in favor of the 3C fit with the highest confidence level as calculated by SQUAW. The contamination of the $\bar{\Lambda}^0$'s is due solely to the K^0's and is estimated to be $\leq 20\%$. The results of this section are summarized in Table II.

C. Weights of the neutral particles

In order to correct for the loss of γ's or V^0's which did not convert or decay in the chamber, we assign to each observed event a weight that is inversely proportional to the probability that the detected particle should be observed in a chosen fiducial volume. The average weights for K_S^0's, Λ^0's, and $\bar{\Lambda}^0$'s backward in the center of mass are 1.38, 1.32, and 1.19, respectively. The average weight for the γ's (both center-of-mass hemispheres) is 9.14.

The experimental loss of γ's with very low or high laboratory momentum can be further corrected by exploiting the forward-backward symmetry of pp collisions in the center-of-mass frame. We found severe losses of γ's with $E_{lab} < 60$ MeV by comparing the attenuation weighted energy distribution of the γ's with that of the γ's which would decay from π^0's of the same distribution as the

TABLE II. Summary of 3C fits for γ, K^0, and Λ^0. The $\bar{\Lambda}^0$'s were treated separately.

	γ	K^0	Λ^0
Unique	2468	180	44
Resolved	222	91	93
Totals	2690	271	137

TABLE III. Topological cross sections at 400 GeV/c.

Prong number	Number observed	Corrected number	Cross section (mb)
3	16		
4	727	743	4.38 ± 0.19
5	13		
6	866	888	5.24 ± 0.22
7	11		
8	831	854	5.04 ± 0.21
9	9		
10	798	802	4.73 ± 0.20
11	12		
12	651	666	3.93 ± 0.18
13	4		
14	473	477	2.81 ± 0.15
15	5		
16	341	342	2.02 ± 0.12
17	4		
18	163	165	0.97 ± 0.08
19	1		
20	87	87	0.51 ± 0.056
21	2	41	0.24 ± 0.038
22	39	23	0.14 ± 0.028
23	0		
24	23	6	0.035 ± 0.015
25	2		
26	6	8	0.047 ± 0.017
27	0		
28	7	3	0.018 ± 0.010
29	0		
30	3		
31	1		

measured π^-'s. These losses were corrected by giving such events a zero weight and doubling the weights of events in the symmetrically reflected region of the center-of-mass momentum space. The efficiency of processing the rest of the γ's in the backward hemisphere is essentially 100%. We made a rapidity dependent correction to the events forward in the center of mass by reflection symmetry in the center of mass. We found this correction can be made independent of multiplicity of the primary interaction. A detailed description of these corrections is given in Ref. 2.

III. CHARGED-PARTICLE CROSS SECTIONS

The charged-particle cross sections were obtained by scanning the film and recording the number of charged prongs (multiplicity) for each event. The number of events with three or more prongs is listed in Table III. Two-prong events are not considered here since the scanning efficiency for them is low (~90%) owing to the loss of short proton tracks caused by the large chamber-to-film demagnification. Events with an odd number of prongs were classified as even prongs according

to the following scheme:

(1) Add one to the multiplicity if the prong number was ≤ 7.

(2) Subtract three[6] from the multiplicity if the prong number was ≥ 9.

The number of events after making this correction is listed in the third column of Table III. The topological cross sections σ_n were calculated by normalizing to the cross section of Ref. 7 for production of four or more prongs.

The topological cross sections are in agreement

TABLE IV. Low-order moments of multiplicity distribution.

	All prongs[a]	≥ 4 prongs
$\langle N_- \rangle$	3.57 ± 0.06	3.89 ± 0.03
$\langle N_-^2 \rangle$	18.44 ± 0.42	20.10 ± 0.31
f_2^{--}	2.14 ± 0.16	1.09 ± 0.10

[a] Assuming an inelastic two-prong cross section of 2.7 ± 0.5 mb as in Ref. 7.

TABLE V. Inclusive topological cross sections.

Prongs	π^0 Events	σ_{π^0} (mb)	K_S^0 Events	$\sigma_{K_S^0}$ (mb)	Λ^0 Events	σ_{Λ^0} (mb)	$\bar\Lambda^0$ Events	$\sigma_{\bar\Lambda^0}$ (mb)
2	103	5.07 ± 0.93	5	0.17 ± 0.12	3	0.10 ± 0.08	0	$\cdots$
4	225	11.49 ± 1.52	15	0.55 ± 0.22	11	0.35 ± 0.15	0	$\cdots$
6	402	18.62 ± 1.89	30	0.98 ± 0.27	20	0.71 ± 0.24	3	0.09 ± 0.07
8	490	21.80 ± 1.98	29	0.93 ± 0.25	28	0.94 ± 0.26	2	0.06 ± 0.06
10	507	21.25 ± 1.82	33	1.00 ± 0.26	18	0.59 ± 0.20	4	0.12 ± 0.09
12	485	22.94 ± 2.13	35	1.21 ± 0.33	12	0.37 ± 0.15	2	0.07 ± 0.07
14	369	15.76 ± 1.63	22	0.80 ± 0.27	11	0.36 ± 0.16	1	0.03 ± 0.03
16	276	11.67 ± 1.35	20	0.63 ± 0.20	8	0.26 ± 0.13	2	0.06 ± 0.06
18	161	7.34 ± 1.17	4	0.12 ± 0.08	4	0.13 ± 0.09	0	$\cdots$
20	78	2.76 ± 0.55	5	0.14 ± 0.09	3	0.10 ± 0.08	0	$\cdots$
22	47	2.08 ± 0.67	3	0.089 ± 0.073	1	0.03 ± 0.03	0	$\cdots$
24	15	0.75 ± 0.36	0	$\cdots$	1	0.03 ± 0.03	0	$\cdots$
26	9	0.34 ± 0.22	0	$\cdots$	0	$\cdots$	0	$\cdots$
28	8	0.27 ± 0.17	0	$\cdots$	0	$\cdots$	0	$\cdots$
30	2	0.18 ± 0.18	0	$\cdots$	0	$\cdots$	0	$\cdots$
Total	3177	142.3 ± 6.2	201	6.61 ± 0.73	120	3.97 ± 0.54	14	0.42 ± 0.16

with those of Ref. 7. Some low-order moments of the multiplicity distribution are presented in Table IV. These quantities are calculated in terms of N_-, the number of negative tracks in an event.

The average number of negative particles per inelastic collision ($\langle N_- \rangle$) increases by approximately 40% when the laboratory momentum changes from 100 to 400 GeV/c. The correlation parameter f_2^{--} $[\equiv \langle N_-(N_- - 1) \rangle - \langle N_- \rangle^2]$ increases rapidly in this momentum range, growing from a value of 0.28 at 102 GeV/c to 2.14 at 400 GeV/c.

IV. CROSS SECTIONS FOR π^0, K^0, Λ^0, and $\bar\Lambda^0$

In this section we consider the following reactions:

(a) $pp \to \pi^0 X$,

(b) $pp \to K_S^0 X$,

(c) $pp \to \Lambda^0 X$,

(d) $pp \to \bar\Lambda^0 X$.
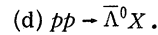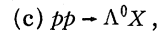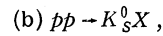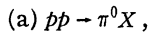
Only particles backward in the center of mass were used in obtaining cross sections for neutral-strange-particle production. Corrections were made for unseen decay modes. The π^0 cross section was obtained from the γ cross section through $\sigma_{\pi^0} = \sigma_\gamma/2$. The inclusive and semi-inclusive cross sections for these reactions are listed in Table V. Figures 1–3 show these cross sections as a function of incident proton laboratory momentum.[8-17]

The π^0 cross section is rising as a function of incident momentum, as predicted by most multiperipheral models (Fig. 1). At the highest energies, however, the cross section appears to deviate from the expected lns behavior.

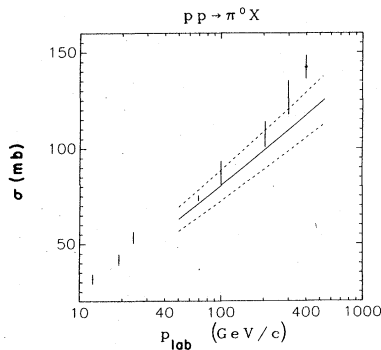The neutral-pion cross section can be compared (curves in Fig. 1) with the charged-pion cross sec-

FIG. 1. Inclusive cross section for π^0 production as a function of incident laboratory momentum. $\diamondsuit$ = this experiment. The solid curve is an estimate (Ref. 18) of $(\sigma_{\pi^+} + \sigma_{\pi^-})/2$. The dashed curves are 10% upper and lower limits of the solid curve.
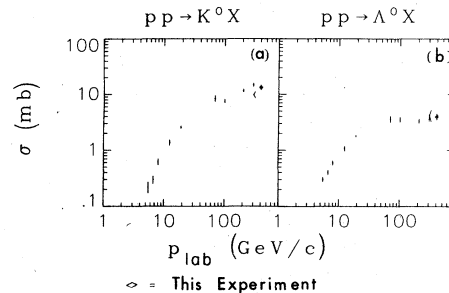

FIG. 2. (a) Inclusive K^0 cross section as a function of incident laboratory momentum. (b) Inclusive Λ^0 cross section as a function of incident laboratory momentum.
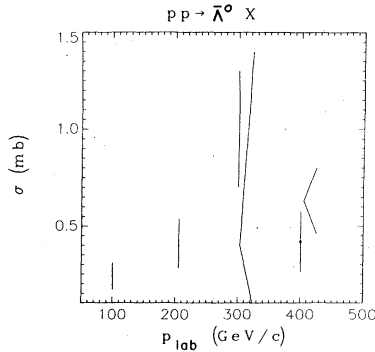
FIG. 3. Inclusive $\bar{\Lambda}^0$ cross section as a function of incident laboratory momentum.

tion ($\sigma_{\pi^+}, \sigma_{\pi^-}$) using the data of Ref. 18. We find $\sigma_{\pi^0}(142.3 \pm 6.2 \text{ mb}) > \sigma_{\pi^+}(128 \text{ mb}) > \sigma_{\pi^-}(107 \text{ mb})$. Since the parametrizations for σ_{π^+} and σ_{π^-} are expected to be accurate only to ~10%, one could argue that σ_{π^0} is consistent with σ_{π^+}. It is definitely inconsistent with σ_{π^-}, however.

In the hundred-GeV range we see that $\sigma_{K_S^0}$ is only slightly energy dependent, in marked contrast to its behavior at lower energies [Fig. 2(a)]. The behavior of σ_{Λ^0} (Ref. 19) [Fig. 2(b)] is similar to that of $\sigma_{K_S^0}$ over most of the momentum range under consideration. However, $\sigma_{K_S^0}$ and σ_{Λ^0} are not related by a simple change of scale since $\sigma_{K_S^0}$ rises faster than σ_{Λ^0}. In addition, σ_{Λ^0} does not show any energy dependence in the hundred-GeV range.

There are four events of the type $pp \to K_S^0 K_S^0 X$ with both K_S^0's backward in the center of mass. These four events correspond to a cross section of 0.16 ± 0.09 mb. Two of these events have $m_{K^0 K^0}$

< 1.1 GeV/c^2, suggesting that a substantial fraction of the K_S^0 pairs are produced near threshold.

The dependence of $\sigma_{\bar{\Lambda}^0}$ (Fig. 3) on incident momentum is uncertain since most bubble-chamber experiments with $P_{lab} > 50$ GeV/c detect fewer than 20 $\bar{\Lambda}^0$'s. What is clear is that $\sigma_{\bar{\Lambda}^0}$ is only a fraction ($\approx$10% for this experiment) of σ_{Λ^0}. Presumably this difference is due to proton fragmentation ($p \to K^+ \Lambda^0$) which can produce Λ^0's but not $\bar{\Lambda}^0$'s.

A question of interest is how much of the $\bar{\Lambda}^0$'s are the result of $\Lambda^0 \bar{\Lambda}^0$ production. In this experiment there are three events with a $\Lambda^0 \bar{\Lambda}^0$ pair, both particles being backward in the center of mass. These three events correspond to a cross section of $\sigma_{\Lambda^0 \bar{\Lambda}^0} = 0.12 \pm 0.07$ mb. A sizable fraction of the $\bar{\Lambda}^0$'s are thus produced in association with a Λ^0. All three pairs are produced in the central region of rapidity and in all cases $|Y_{\Lambda^0} - Y_{\bar{\Lambda}^0}| < 1$.

In summary, we have seen that the neutral-strange-particle cross sections are at most only slightly energy dependent in the hundred-GeV range, while the π^0 cross section is rising at least as fast as lns.

V. AVERAGE NUMBER OF PARTICLES PER INELASTIC COLLISION

The average number of particles per inelastic collision for reactions (a)–(c), $\langle \pi^0 \rangle$, $\langle K_S^0 \rangle$, and $\langle \Lambda^0 \rangle$, are listed in Table VI. Figures 4 and 5 show the dependence of these quantities on incident momentum.

The average number of π^0 per inelastic collisions, $\langle \pi^0 \rangle$, is a rising function of incident momentum P_{lab}. A comparison is made to the $\ln P_{lab}$ fit

TABLE VI. Average number of π^0, K_S^0, Λ^0, $\bar{\Lambda}^0$ per inelastic collision.

| Prongs	π^0 Events	$\langle \pi^0 \rangle$	K_S^0 Events	$\langle K_S^0 \rangle$	Λ^0 Events	$\langle \Lambda^0 \rangle$	$\bar{\Lambda}^0$ Events	$\langle \bar{\Lambda}^0 \rangle$
2	103	1.90 ± 0.24	5	0.064 ± 0.032	3	0.037 ± 0.022	0	$\cdots$
4	225	2.53 ± 0.23	15	0.12 ± 0.03	11	0.076 ± 0.02	0	$\cdots$
6	402	3.54 ± 0.24	30	0.19 ± 0.04	20	0.13 ± 0.03	3	0.017 ± 0.010
8	490	4.32 ± 0.25	29	0.18 ± 0.03	28	0.19 ± 0.04	2	0.011 ± 0.008
10	507	4.48 ± 0.24	33	0.21 ± 0.04	18	0.13 ± 0.03	4	0.026 ± 0.013
12	485	5.92 ± 0.35	35	0.31 ± 0.06	12	0.10 ± 0.03	2	0.017 ± 0.012
14	369	5.78 ± 0.36	22	0.29 ± 0.07	11	0.13 ± 0.04	1	0.011 ± 0.011
16	276	5.96 ± 0.41	20	0.32 ± 0.07	8	0.13 ± 0.05	2	0.030 ± 0.021
18	161	7.34 ± 0.72	4	0.12 ± 0.06	4	0.13 ± 0.06	0	$\cdots$
20	78	5.34 ± 0.59	5	0.27 ± 0.11	3	0.20 ± 0.12	0	$\cdots$
22	47	8.29 ± 1.78	3	0.35 ± 0.20	1	0.12 ± 0.12	0	$\cdots$
24	15	5.68 ± 1.63	0	$\cdots$	1	0.22 ± 0.22	0	$\cdots$
26	9	10.95 ± 3.16	0	$\cdots$	0	$\cdots$	0	$\cdots$
28	8	6.01 ± 2.03	0	$\cdots$	0	$\cdots$	0	$\cdots$
30	2	9.06 ± 4.63	0	$\cdots$	0	$\cdots$	0	$\cdots$
Total	3177	4.43 ± 0.10	201	0.20 ± 0.02	120	0.12 ± 0.01	14	0.013 ± 0.003
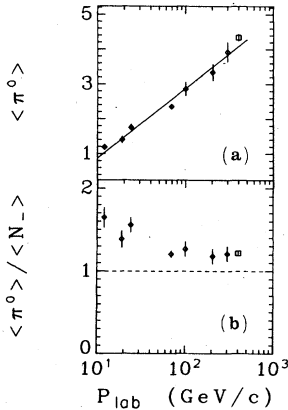
FIG. 4.(a) Average number of π^0's per inelastic collision as a function of incident laboratory momentum. The curve (Ref. 11) is a fit to data other than this experiment and that at 69 GeV/c. (b) The ratio $\langle\pi^0\rangle/\langle N_-\rangle$ as a function of incident laboratory momentum.

of Ref. 8, $\langle\pi^0\rangle = -1.13 + 0.87 \ln P_{lab}$. The two points with the smallest errors, ours and that at 69 GeV/c, are not part of their fit, and deviate substantially from the $\ln P_{lab}$ behavior.[20] As a matter of fact, the points above 69 GeV definitely rise faster than the indicated straight line. A similar behavior is well known in the P_{lab} dependence of average multiplicity, $\langle N_-\rangle$. One is tempted to make other functional fits to $\langle\pi^0\rangle$ as is done in the case of $\langle N_-\rangle$. However, the errors of the $\langle\pi^0\rangle$ values do not warrant such an attempt. Rather, one can ask whether the P_{lab} dependence of $\langle\pi^0\rangle$ is the same as $\langle N_-\rangle$. To answer that question we plot the ratio $\langle\pi^0\rangle/\langle N_-\rangle$ as function of P_{lab}. In Fig. 4(b) we see this ratio is indeed a *constant* at Serpukhov and Fermilab energies. The weighted average for these high-energy points is 1.22 ± 0.02.

Next we turn our attention to the average number of particles for fixed N_- ($\langle A\rangle_-$). By N_- we mean
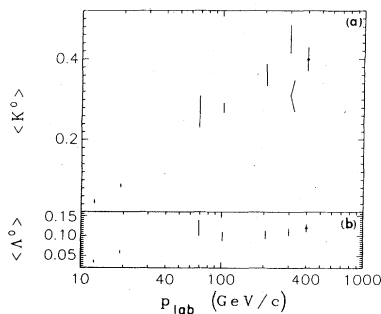

FIG. 5.(a) Average number of K^0's per inelastic collision as a function of incident laboratory momentum. (b) Average number of Λ^0's per inelastic collision as a function of incident laboratory momentum.
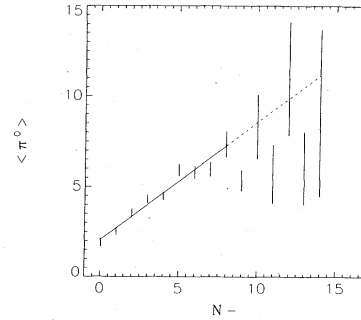

FIG. 6. Average number of π^0's as a function of the number of negative particles (N_-) in an event. The solid line is a least-squares fit to $\langle\pi^0\rangle = A + BN_-$, using the first points. The dashed curve is an extension of the solid curve.

the number of negative particles in the event. In Figs. 6–8 we plot $\langle\pi^0\rangle_-$, $\langle K_S^0\rangle_-$, and $\langle\Lambda^0\rangle_-$. The behavior of $\langle A\rangle_-$ is different for mesons and baryons.

For the π^0's and K_S^0's $\langle A\rangle_-$ increases with increasing N_-. Both $\langle\pi^0\rangle_-$ and $\langle K^0\rangle_-$ can be represented by $\langle A\rangle_- = a + bN_-$. The results of the fits are given in Table VII. In contrast to the mesons, $\langle\Lambda^0\rangle_-$ is rather flat for $N_- \geqslant 3$.

The strong dependence of $\langle\pi^0\rangle_-$ on N_- suggests that for some large fraction of the time, the observed π^0's and π^-'s are the products of the decay of some higher-mass object. This object might be a vector meson of a "blob" of indefinite mass but fixed isospin. The concept of the massive blob is similar to that of proton diffraction (e.g., $p \rightarrow N\pi^+$) where the quantum numbers of the $N\pi^+$ system are fixed but the mass of the system is not. It is also possible that the observed correlation between the π^0's and π^-'s might be accounted for by some statistical process.

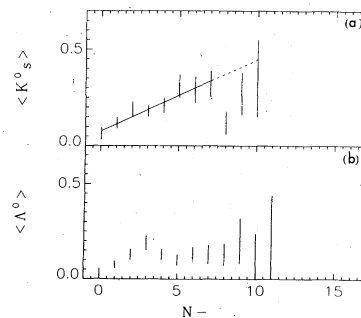In Fig. 8 the predictions for the $\langle\pi^0\rangle_-$ vs N_- for

FIG. 7.(a) Average number of K_S^0's as a function of N_-. The solid curves are a least-squares fit to $\langle K_S^0\rangle = A + BN_-$ using the first eight points. The dashed curve is an extension of the solid curve. (b) Average number of Λ^0's as a function of N_-.

five models[21-26] of pion production are compared with the experimental data. The models considered are

(1) "π" model—single-pion production,
(2) "ϵ" model—production of $\pi^+\pi$, $\pi^0\pi^0$, $I=0$ pairs
(3) "ρ" model—production of $\pi^+\pi^-$, $\pi^+\pi^0$, $\pi^-\pi^0$, $I=1$ pairs
(4) "ω" model—production of $\pi^+\pi^-\pi^0$, $I=0$ triplets
(5) "critical-fluid" model—a thermodynamic model.

All of the models considered predict a rise in the $\langle\pi^0\rangle_-$ as a function of N_-. Only the critical-fluid model is in good agreement with the data, however. The ϵ model provides a fair description of the data if the errors associated with the predicted points are taken into consideration. The remaining three models (π,ρ,ω) are inconsistent with the data. A more detailed discussion of these models is given in Sec. VII.

VI. PRODUCTION of π^0, $\eta(548)$, $\omega(783)$, Σ^0, and $\overline{\Sigma}^0$.

In Fig. 9(a), the invariant-mass distribution for γ pairs is displayed. A strong π^0 signal is present. In order to show more clearly the π^0 signal and cut out some of the low-mass backgrounds ($M_{\gamma\gamma}\lesssim 120$ MeV), a minimum $\gamma\gamma$ opening angle cut was made.[27] In addition, only events that have their primary vertex in the first half of the chamber were used. This fiducial cut was made to minimize the large fluctuations in the weights of the γ pairs. In Fig. 9(b), the weighted mass distribution is shown. In Figs. 9(c) and 9(d) the unweighted and weighted mass distribution for γ pairs fitting (using SQUAW) the hypothesis $\pi^0 \to \gamma\gamma$ are presented. Using

the events in Figs. 9(c) and 9(d) with $125 \leqslant M_{\gamma\gamma} < 145$ for the π^0 signal, we calculate a cross section, σ_{π^0}, of 138 ± 15 mb. This is consistent with the value of 142 ± 6 mb which was obtained assuming $\sigma_{\pi^0} = \frac{1}{2}\sigma_\gamma$.

In Figs. 9(a) and 9(b), there is no evidence for $\eta(548)$ production. An upper limit (at the 90% confidence level) for the ratio $\eta(548)/\pi^0$ can be found using the fitted π^0 events [Figs. 9(c) and 9(d)]. We obtain

$$\eta(548)/\pi^0 < 5\% ,$$

and

$$\sigma_\eta(548) < 7 \text{ mb} ,$$

90% confidence level all decay modes included.

The search for $\omega(783)$ production was made only in events with $\leqslant 10$ prongs. All tracks were assumed to be pions unless they were identified otherwise. In order to ensure that the $\pi^+\pi^-\pi^0$ combination was well measured, we use only events (unless otherwise mentioned) which satisfy

$$\frac{\delta M_{\pi^+\pi^-\pi^0}}{M_{\pi^+\pi^-\pi^0}} < 2\% , \quad \delta M = \text{error in mass}, \quad M = \text{mass},$$

calculated by SQUAW.

In Figs. 10(a) and 10(b) the unweighted and weighted mass distribution of all (the above-mentioned cut is not imposed) γ pairs in events with $\leqslant 10$ prongs is displayed. The events that fit the reaction $\pi^0 \to \gamma\gamma$ (using SQUAW) and meet the above mentioned error cut are shown in Figs. 10(c) (unweighted) and 10(d) (weighted).

The invariant-mass distribution for $\pi^+\pi^-\pi^0$ triplets is shown in Fig. 11. There is no obvious $\omega(783)$ signal present. In order to search further for this signal, we have also used the variable[28] $\lambda \equiv (Q/Q_{max})^2$ where Q is the matrix element of the $\omega(783)$. For a 1^- particle, $Q^2 = |\overline{K}_1 \times \overline{K}_2|^2$, where $\overline{K}$ is the momentum of a decay production in the rest frame of the $\omega(782)$ and Q_{max} is the largest value of Q. Specifying a value for λ is equivalent to specifying a region in a Dalitz plot. For pure
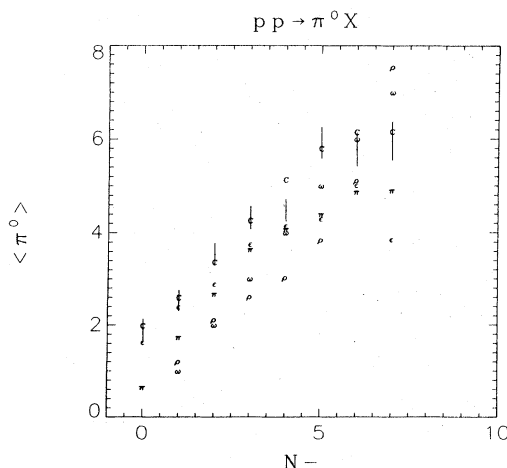

$$p\,p \to \pi^0 X$$

FIG. 8. The predictions for the $\langle\pi^0\rangle$ as a function of N_- for the π, ϵ, ρ, ω, and critical-fluid (C) model.

TABLE VII. Results of the fit to $\langle A \rangle_- = a + bN_-$.

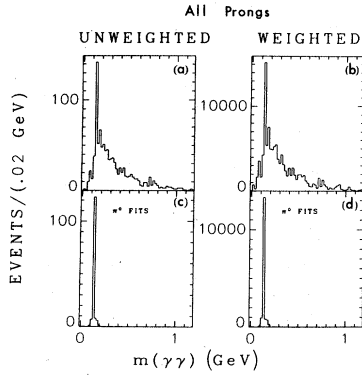|	a	b	χ^2/DOF
π^0	2.05 ± 0.15	0.65 ± 0.04	1.39
K_S^0	0.078 ± 0.022	0.037 ± 0.007	0.34

FIG. 9. Invariant-mass distribution for $\gamma\gamma$ pairs. (a) All combinations unweighted. (b) All combinations weighted. (c) Satisfying π^0 hypothesis unweighted. (d) Satisfying π^0 hypothesis weighted.

ω decays, with Dalitz plot governed by the $J^P = 1^-$ matrix element, it is expected that $\frac{3}{4}$ of the events have $\lambda \geqslant 0.5$. A random combination of $\pi^+\pi^-\pi^0$ gives equal amounts of events below and above $\lambda = 0.5$. A histogram of λ for events with $735 \leqslant M_{\pi^+\pi^-\pi^0}$ $\leqslant 835$ MeV is shown in Fig. 12. There is no excess of events with $\lambda \geqslant 0.5$ and we conclude that there is little if any $\omega(783)$ present. The upper limit (90% confidence level) for $\omega(783)$ production is $\omega(783)/\pi^0 < 4.8\%$ or $\sigma_{\omega(783)} < 3$ mb. We remind the reader that these are based on events with fewer than 11 prongs. All decay modes were included and corrections were made for events with $\delta M/M > 2\%$.

The cross sections for Σ^0 and $\overline{\Sigma}^0$ production are obtained using events that fit (using SQUAW) the following reactions:

(a) $\Sigma^0 \rightarrow \Lambda^0$ γ e^+e^-
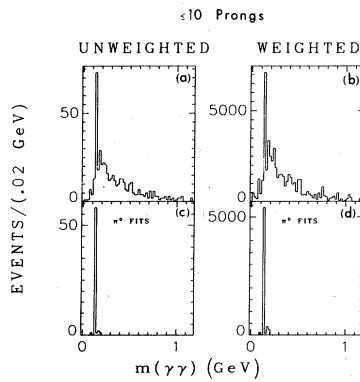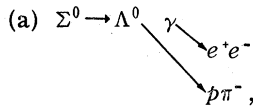 $p\pi^-$,

FIG. 10. Invariant-mass distribution for $\gamma\gamma$ pairs in ten-or-less-prong events. (a) All combinations unweighted. (b) All combinations weighted. (c) Satisfying π^0 hypothesis unweighted. (d) Satisfying π^0 hypothesis weighted.
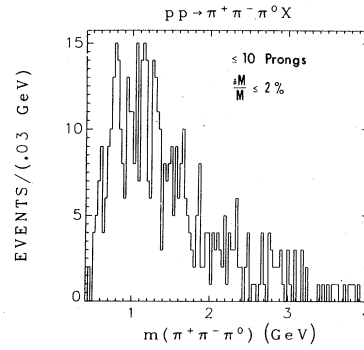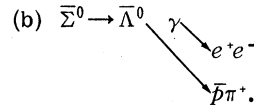

FIG. 11. Invariant-mass distribution for $\pi^+\pi^-\pi^0$ triplets.

(b) $\overline{\Sigma}^0 \rightarrow \overline{\Lambda}^0$ γ e^+e^-
                    $\overline{p}\pi^+$.

There is one event above background for each of these reactions, giving

$$\sigma_{\Sigma^0} = 0.26 \text{ mb},$$

$$\sigma_{\overline{\Sigma}^0} = 0.22 \text{ mb}.$$

The above cross sections are for both center-of-mass hemispheres, and include the branching ratio of unseen decay modes.

In Ref. 16, a cross section of 1.14 mb for charged $Y^*(1385)$ ($\rightarrow \Lambda^0\pi$ only) production was obtained. This fact, coupled with the estimate obtained for σ_{Σ^0}, suggests that $\geqslant \frac{1}{4}$ of the detected Λ^0's are decay products of a higher-mass state.

VII. INCLUSIVE TWO-BODY CORRELATIONS

In this section correlations between neutral and charged pions will be studied and compared to the predictions of the five previously mentioned models. In particular, we examine the behavior of the Mueller correlation parameters:

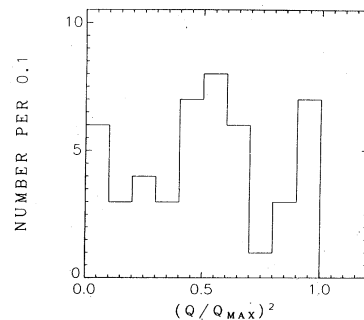$$f_2^{--} = \langle N_-(N_- - 1) \rangle - \langle N_- \rangle^2 ,$$

FIG. 12. Distribution of $\lambda \equiv (Q/Q_{\text{max}})^2$.

TABLE VIII. Two-body correlation moments.

f_2^{--}	2.14 ± 0.16
f_2^{0-}	3.28 ± 0.31
f_2^{00}	4.81 ± 1.40

$$f_2^{0-} = \langle N_0 N_- \rangle - \langle N_0 \rangle \langle N_- \rangle \;,$$

$$f_2^{00} = \langle N_0 (N_0 - 1) \rangle - \langle N_0 \rangle^2 \;.$$

Assuming $N_0 = N_\gamma / 2$, we can rewrite f_2^{00} as

$$f_2^{00} = \tfrac{1}{4} [\langle N_\gamma (N_\gamma - 1) \rangle - \langle N_\gamma \rangle^2] - \tfrac{1}{4} \langle N_\gamma \rangle$$

$$= \tfrac{1}{4} f_2^{\gamma\gamma} - \tfrac{1}{4} \langle N_\gamma \rangle \;.$$

Table VIII lists the values of f_2^-, f_2^{0-}, and f_2^{00}. The ordering of the parameters $f_2^{--} < f_2^{0-} < f_2^{00}$ implies that π^0's are more correlated than π^-'s. The semi-inclusive scaling law of Ref. 29 leads to the prediction that at high energies, $f_2^{--} > f_2^{0-}$. The data do not support this prediction.

The incident-momentum dependence[7-16,30-33] of the three correlation parameters is displayed in Figs. 13(a)–13(c). All parameters are increasing with increasing incident momentum.

In order to explain the observed correlations at 400 GeV/c, we now consider the five models of pion production. These models allow one to calculate f_2^{0-} and f_2^{00} in terms of the well-measured quantities, f_2^{--} and $\langle N_- \rangle$. The results are displayed in Figs. 14(a) and 14(b). Of the models considered, the critical-fluid model shows the best agreement
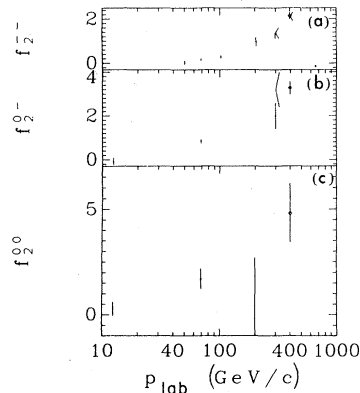

FIG. 14.(a) Comparison of f_2^{0-} with predictions of ω, ρ, π, ϵ, and critical-fluid (C) model. (b) Comparison of f_2^{00} with predictions of ω, ρ, π, ϵ, and critical-fluid (C) model.

with the data. No model having only one type of cluster with definite isospin fits all data. It would be possible, however, to fit the data with a model incorporating two or more clusters of definite isospin (e.g., a "$\rho + \epsilon$" model).

VIII. CONCLUSION

We have presented results on charged- and neutral-particle production from pp collisions at 400 GeV/c. The main results are the following:

(a) Inclusive and semi-inclusive measurements of π^0, K_S^0, Λ^0, $\bar{\Lambda}^0$, Σ^0, and $\bar{\Sigma}^0$ have been made. The π^0 cross section is rising at least as fast as $\ln s$. The K_S^0 cross section also appears to increase at Fermilab energies. In contrast, the Λ^0 cross section is constant at Fermilab energies. The average number of π^0's and K_S^0's increases as a function of the number of negative particles in an event. No such dependence is found for the Λ^0's.

(b) From the events with two or more converted γ's, upper limits are calculated for inclusive $\eta^0(548)$ production and, for events with fewer than 11 prongs, $\omega^0(783)$ production.

(c) Neutral- and charged-pion correlations were studied in terms of $\langle \pi^0 \rangle_-$ and the Mueller moments, f_2^{--}, f_2^{0-}, and f_2^{00}. Predictions from five models of pion production were compared with the data. Of these, only the critical-fluid model is in good agreement with the data.

ACKNOWLEDGMENTS

FIG. 13.(a) f_2^{--} as a function of laboratory momentum. (b) f_2^{0-} as a function of laboratory momentum. (c) f_2^{00} as a function of laboratory momentum.
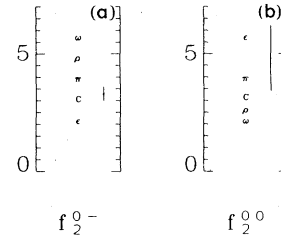
*Present address: Laboratory of Nuclear Studies, Cornell University, Ithaca, N.Y. 14853.

[1]See, for example, J. Whitmore, Phys. Rep. **27**, 187 (1976).

[2]For further details of this experiment see R. Kass, Ph.D. thesis, University of California, Davis, 1978 (unpublished), and R. D. Kass *et al.*, in *Proceedings of the XIX International Conference on High Energy Physics, Tokyo, 1978,* edited by S. Homma, M. Kawaguchi, and H. Miyazawa (Phys. Soc. of Japan, Tokyo, 1979).

[3]J. Erwin *et al.*, Nucl. Instrum. Methods **148**, 403 (1978).

[4]W. Michael *et al.*, Report No. UCID-3880, 1977 (unpublished).

[5]The coordinate system is such that the beam is in the positive X direction, Z is vertical, and $\vec{Y} = \vec{Z} \times \vec{X}$.

[6]The average multiplicity of secondaries is ~ 4.

[7]C. Bromberg *et al.*, Phys. Rev. Lett. **31**, 1563 (1973); **32**, 83(E) (1974).

[8]K. Jaeger *et al.*, Phys. Rev. D **11**, 1756 (1975). Data at 12.4 GeV/c.

[9]H. Bøggild *et al.*, Nucl. Phys. **B72**, 221 (1974). Data at 19 GeV/c.

[10]V. Blobel *et al.*, Nucl. Phys. **B69**, 454 (1972). Data at 12 and 24 GeV/c.

[11]M. Boratav *et al.*, Nucl. Phys. **B111**, 529 (1976); H. Blumenfeld *et al.*, Phys. Lett. **45B**, 528 (1973). Data at 69 GeV/c.

[12]M. Alston-Garnjost *et al.*, Phys. Rev. Lett. **35**, 142 (1975). Data at 100 GeV/c.

[13]J. W. Chapman *et al.*, Phys. Lett. **47B**, 465 (1973). Data at 102 GeV/c.

[14]K. Jaeger *et al.*, Phys. Rev. D **11**, 2405 (1975). Data at 205 GeV/c.

[15]A. Sheng *et al.*, Phys. Rev. D **11**, 1733 (1975). Data at 300 GeV/c.

[16]F. T. Dao *et al.*, Phys. Rev. Lett. **30**, 1151 (1973). Data at 303 GeV/c.

[17]H. Kichimi *et al.*, Phys. Lett. **72B**, 411 (1978). Data at 405 GeV/c.

[18]M. Antinucci *et al.*, Lett. Nuovo Cimento **6**, 121 (1973). The authors parametrize the average number of particles per inelastic collision as a function of s. For charged pions they obtain

$$\langle \pi^+ \rangle = -1.7 \pm 0.3 + (0.84 \pm 0.07) \ln s + \frac{(1.0 \pm 0.5)}{\sqrt{s}} \ ,$$

$$\langle \pi^- \rangle = -2.6 \pm 0.2 + (0.87 \pm 0.05) \ln s + \frac{(2.7 \pm 0.4)}{\sqrt{s}}.$$

This parametrization is estimated to be accurate to within 10%. The cross sections can be calculated using, e.g., $\sigma_{\pi^+} = \langle \pi^+ \rangle \, \sigma_{in}$ with σ_{in} taken from Ref. 10. Using this prescription, we obtain

$$\sigma_{\pi^+} = 128 \text{ mb}, \quad \sigma_{\pi^-} = 107 \text{ mb}.$$

[19]Some of these Λ^0 ($\bar{\Lambda}^0$) may be decay products of Σ^0's ($\bar{\Sigma}^0$'s).

[20]J. Whitmore, Phys. Rep. **10C**, 273 (1974). Whitmore fits the $\langle \pi^0 \rangle$ to $\langle \pi^0 \rangle = -0.82 \pm 0.79$ in P_{lab}. The value of $\langle \pi^0 \rangle$ obtained by this experiment deviates even more from this line than from that of Ref. 11.

[21]R. C. Arnold and G. H. Thomas, Phys. Lett. **47B**, 371 (1973).

[22]G. H. Thomas, Phys. Rev. D **8**, 3042 (1973).

[23]D. Drijard and S. Pokorski, Phys. Lett. **43B**, 509 (1973).

[24]E. L. Berger *et al.*, Phys. Rev. D **7**, 1412 (1973).

[25]D. Horn and A. Schwimmer, Nucl. Phys. **B52**, 627 (1973).

[26]P. Grassberger and H. I. Miettinen, Nucl. Phys. **B82**, 26 (1974).

[27]For a π^0 of laboratory energy E, the minimum opening angle (ϕ) between the two γ's is

$$\cos(\phi/2) = \left[1 - \left(\frac{M_{\pi^0}}{E} \right)^2 \right]^{1/2}, \quad M_{\pi^0} = \text{rest mass of } \pi^0.$$

[28]Trilling-Goldhaber Group, Internal Memo No. 62, 1963 (unpublished).

[29]F. T. Dao and J. Whitmore, Phys. Lett. **B46**, 252 (1973).

[30]V. V. Ammosov *et al.*, Phys. Lett. **B42**, 519 (1972). Data at 50 and 69 GeV/c.

[31]G. Charlton *et al.*, Phys. Rev. Lett. **29**, 515 (1972). Data at 205 GeV/c.

[32]A. Firestone *et al.*, Phys. Rev. D **10**, 2080 (1974). Data at 300 GeV/c.

[33]F. T. Dao *et al.*, Phys. Rev. Lett. **29**, 1627 (1972). Data at 303 GeV/c.